Modeling of Wave Driven Molecular (H_2, N_2, N_2–Ar) Discharges as Atomic Sources

Carlos M. Ferreira, Elena Tatarova, Vasco Guerra, Boris F. Gordiets, Júlio Henriques, Francisco M. Dias, and Mário Pinheiro

***Abstract*—Microwave H_2, N_2, and N_2–Ar discharges driven by traveling surface waves are investigated as sources of ground state N(^{4}S), H(1s) atoms. The dissociation kinetics is discussed in the framework of theoretical models based on a self-consistent treatment of the main discharge balances, wave electrodynamics and plasma-wall interactions. It is shown that the number density of hydrogen H(1s) atoms depends heavily on the wall conditions at low pressure conditions. The kinetics of N(^{4}S) and metastable N(^{2}D) and N(^{2}P) atoms and of the molecular $N_2(A^3\Sigma_u^+)$ metastable state in a pure N_2 discharge are shown to be strongly coupled. One possible way to control and to enhance nitrogen dissociation is the use of an N_2–Ar mixture. The increase in dissociation degree of N_2 molecules at high Ar fractional concentration can be attributed to dissociative recombination between electrons and N_2^+ positive ions. The predicted results for the atomic density are compared with emission spectroscopy data.**

***Index Terms*—Argon, dissociation, hydrogen, microwave discharge, modeling, nitrogen, plasma-wall, spectroscopy.**

I. Introduction

THE INTEREST in nonequilibrium molecular plasmas generated by traveling surface waves (large scale long plasma columns or flat plasmas) is motivated by the advantageous properties of these sources regarding plasma based technologies [1]–[4]. Surface wave (SW) discharges operating at microwave frequencies have flexible operation and are characterized by high number densities of active neutral species. In fact, of major importance are long-lived species such as ground state atoms. For example, nitrogen atoms are important precursors in surface treatment processes while hydrogen atoms constitute efficient etching species. Moreover the design and development of nitrogen atom sources could be essential for the synthesis of gallium nitride (GaN), a wide bandgap semiconductor whose properties have revolutionized microelectronics and optoelectronic industries. Some peculiar plasma devices involve remote plasmas; such setups use the energy transferred in a tubular discharge which is carried by the flow to the processing reactor [3], [4]. In this case, nitrogen atoms are present in the postdischarge mainly due to their axial transport. Therefore, the optimization of such a system is inevitably coupled to the discharge source operation since the conditions at the end of the source determine the initial conditions for the postdischarge.

The degree of molecular dissociation strongly influences the whole discharge kinetics, thus the study of dissociation kinetics is important on a fundamental basis too. Furthermore, the volume and surface kinetics in discharges operating in molecular gases are strongly coupled. As is well known [5], the surface reactions, particularly those involving dissociated atoms, play a crucial role in the whole discharge kinetics. Wall reactions determine the probabilities of atomic reassociation and of destruction of metastable species, and thus affect the concentration of atoms and other species in the plasma bulk. For example, wall reassociation of H(1s) appears to be an important surface process at low-pressure conditions [6], [7]. Concerning nitrogen discharges, the kinetics of atoms is usually oversimplified in the theoretical models insofar as the kinetics of the atomic metastable is not included even though metastable and ground state atoms are strongly coupled. Previous theoretical models describing SW discharges have disregarded this important problem [8]–[11].

This paper is concerned with the modeling of surface wave driven discharges in hydrogen, nitrogen and N_2–Ar mixtures having in view a detailed analysis of the processes of molecular dissociation, and the establishment of theoretical models, which may be instrumental for discharge optimization regarding the production of atomic species. The basic point of interest here is the analysis of the collisional and transport processes responsible for the balance between creation and loss of atoms as well as the influence of the wall on this balance. In wave driven discharges, all the balances governing discharge production (such as the ionization, heavy particle and thermal balances) are strongly correlated and inevitably coupled with the wave electrodynamics [8]. For this reason, the processes of molecular dissociation must be analyzed taking into account these inherent interdependences along with the effects of plasma-wall interactions.

In the present work, molecular dissociation is studied on the basis of self-consistent models, which include coupled equations for the plasma bulk describing the kinetics of free electrons, the vibrational kinetics of electronic ground state molecules $[N_2(X^1\Sigma_g^+, v), H_2(X^1\Sigma_g^+, v)]$, the kinetics of excited electronic states of molecules $[H_2(a^3\Sigma_g^+, c^3\Pi_u, e^3\Sigma_u^+, d^3\Pi_u^-, B^1\Sigma_u^+, c^1\Pi_u)]$, $[N_2\ (A^3\Sigma_u^+,\ a'^1\Sigma_u^-,\ B^3\,\Pi_g,\ C^3\,\Pi_u,\ a^1\,\Pi_g,\ w^1\Delta_u)]$ and atoms [H(1s), N(^{4}S)], the chemical kinetics of ions $[N_2^+, N_4^+, H^+, H^-, Ar^+]$, the gas thermal balance and the charged particle balance (the latter determines discharge sustaining field). The equations for wave dispersion and

Manuscript received November 1, 2002; revised February 17, 2003.

C. M. Ferreira, E. Tatarova, V. Guerra, J. Henriques, F. M. Dias, and M. Pinheiro are with the Centro de Física dos Plasmas, Instituto Superior Técnico, 1049-001 Lisboa, Portuga (e-mail: e.tatarova@ist.utl.pt).

B. Gordiets is with the Lebedev Physical Institute of the Russian Academy of Sciences, 117924 Moscow V-333, Russia.

Digital Object Identifier 10.1109/TPS.2003.815481

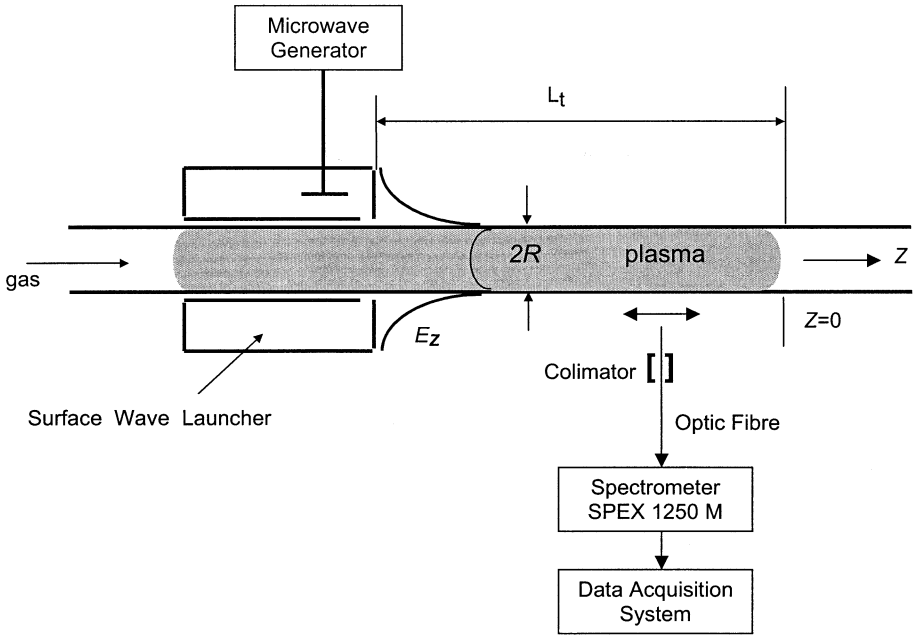

Fig. 1. Experimental setup.

wave power balance are further incorporated in the system of equations.

A detailed analysis of the dissociation kinetics in H_2, N_2, and N_2–Ar discharge is presented. In particular, the important aspect of plasma-wall interaction is addressed. It is shown that the concentration of H(1s) atoms in pure H_2 discharges is strongly influenced by the wall loss probability, which in turn depends heavily on the wall conditions, in particular on the wall temperature. It is further shown that, the volume kinetics of metastable atoms and their interactions with the wall have a significant influence on the dissociation processes in nitrogen discharges. In the N_2–Ar discharge, Ar atoms strongly influence the dissociation processes of nitrogen molecules as a result of the contribution of dissociative recombination between electrons and N_2^+ ions. The theoretical predictions for the ground state atom density are compared with emission spectroscopy data.

The organization of this paper is as follows. In Section II we review some aspects related to the basic features of traveling wave sustained discharges and the self-consistent modeling of such systems. Sections III is devoted to the detailed analysis of the molecular dissociation of discharges operating in H_2, N_2, and N_2–Ar. Finally, in Section IV we discuss the basic results and conclusions of this work.

II. Basic Features and Self-Consistent Modeling of Traveling Surface Wave Sustained Discharges

Surface waves are guided waves, which travel along the interface between two media, for example a plasma and a dielectric. The waves are called surface waves because their field amplitudes have a maximum at the plasma-dielectric interface and decay both in the plasma and the air away from the boundary (see Fig. 1). Discharges driven by surface waves have an extended active zone of operation outside the launcher because the plasma is sustained by a wave which simultaneously propagates and creates its own propagation structure [12]. The wave power P is progressively absorbed by the free plasma electrons, which dissipate this power in collisions with the gas particles. Thus the wave power decreases along the discharge and this causes a decrease of the electron density and a change in the wave propagation characteristics along the wave path. The energy transferred from the electrons to the gas particles is subsequently redistributed by numerous elementary processes among the translational (gas temperature) and internal (vibrational, rotational and electronic) degrees of freedom of the heavy particles. Thus, there is a strong coupling between bulk plasma kinetics, wave electrodynamics and wall conditions. Inhomogeneous wave-to-plasma power transfer results in axial variation of all discharge quantities.

The following situation is considered in the present article. The plasma column is sustained by an azimuthally symmetric (TM mode, $m = 0$) surface wave at a microwave frequency $f = \omega/2\pi$ (500 MHz and 2.45 GHz) in a cylindrical dielectric tube with permittivity ε_d and internal radius R (Fig. 1). The wave field components in cylindrical geometry are E_r, E_z, and H_ϕ. The expressions for the field components are well known and can be found elsewhere [8]. The z coordinate is directed along the tube axis and the wave propagates along z with wave vector $\mathbf{k} = \alpha + i\beta$ (β and α are the axial wave number and the attenuation coefficient, respectively). As the wave propagates and creates its own propagating structure, the wave power flow decreases since its power is progressively absorbed by the electrons. Therefore, the gas is excited, ionized, dissociated and heated. Three important interrelated aspects of discharge physics must be investigated self-consistently, namely [9], [10]:

1) axial variation of different steady-state discharge balances—electron and heavy particle balances, electron energy balance, gas thermal balance, etc.;
2) characteristics of the surface wave propagation along the generated inhomogeneous plasma column, i.e., axial vari-

ation of wave dispersion characteristics and wave power balance;

3) plasma-wall interaction resulting in an axial change of the interface conditions, i.e., the conditions at the wall.

For a self-consistent modeling, the input parameters are the usual externally controlled ones: gas pressure, wave frequency, tube radius, and the power delivered to the launcher or the electron density at the position of the launcher.

It is beyond the scope of this paper to discuss all the processes occurring in the molecular plasmas considered. In this section we will only address a number of important issues for the understanding of the discharge basic workings and in order to briefly describe the set of equations used. These equations are strongly coupled and have been solved altogether in a consistent way. Since only the axial variations in the discharge properties, and not the radial ones, are of concern here, the plasma column is assumed to be radially homogeneous for simplicity. Under the conditions considered, the wave electric field penetrates into the whole plasma cross section (see Fig. 1), therefore there is power absorption across the whole plasma. Although the approach used is likely to introduce some errors in the description of wave propagation and electron kinetics, it nevertheless enables one to deal self-consistently with the coupling between kinetic and electrodynamic aspects. The above system of equations is discussed below.

A. Particle Kinetics

1) Kinetics of Plasma Electrons: The electron energy distribution function (EEDF) of free plasma electrons is determined by solving the homogeneous, quasistationary electron Boltzman equation. The range of applicability of this approximation for surface wave produced molecular plasma is discussed in [12]. The quasistationary approach is valid inasmuch as the frequency of the applied HF field is much higher than the characteristic frequency of electron energy relaxation. Further, under the present conditions, the electrons are not radially in equilibrium with the local reduced electric field at each radial position; the EEDF is rather determined by some radially averaged value of the reduced electric field $E(z)/N(z)$—at a given axial position z. This radially averaged value is called the maintaining field at a given z, which is determined by the charged particles balance (see below). Assuming the anisotropy caused by spatial inhomogeneities and the field to be sufficiently small, the electron velocity distribution is approximated by the usual two-term expansion in spherical harmonics [13]. Inelastic electron collisions of the first and the second kind and electron–electron collisions are accounted for. Since vibrationally excited molecules in N_2 and H_2 discharges constitute an appreciable fraction of the total molecular population, the EEDF is generally a functional of the vibrational distribution function (VDF) of the electronic ground state of $H_2(X^1\Sigma_g^+, v)$ and $N_2(X^1\Sigma_g^+, v)$ molecules. The explicit form of electron Boltzmann equation used for calculations can be found in [14]. The electron cross sections used are the same as in [6], [7], and [15] for H_2 and as in [8]–[10], [14] for N_2 and Ar. The reader should refer to these works for more details concerning electron kinetics description.

The electron transport parameters and the rate coefficients, as calculated from the EEDF, are functions of the reduced HF electric field $E(z)/N(z)$ ($N(z)$ is the total density of the neutrals and $E(z) = \sqrt{E_r^2(z) + E_z^2(z)}$ where $E_r(z)$ and $E_z(z)$ are the radially averaged wave electric field components in the plasma at a given axial position z) sustaining the discharge.

2) Heavy Particle Kinetics: The population of $H_2(X^1\Sigma_g^+, v)$ and $N_2(X^1\Sigma_g^+, v)$ vibrational levels have been determined from the usual coupled system of master equations taking into account (i) vibrational excitation and de-excitation by electron collisions (e-V processes); (ii) vibration-vibration (V-V) exchanges; (iii) vibration-translation (V-T) exchanges in collisions of $N_2(X^1\Sigma_g^+, v)$ with N_2, N and Ar, and of $H_2(X^1\Sigma_g^+, v)$ with H_2, H; (iv) one-quantum energy exchange in collisions of $N_2(X^1\Sigma_g^+, v)$ and $H_2(X^1\Sigma_g^+, v)$ with the wall. Note that only single—quantum transition, which are the most likely ones, are usually considered in the (V-V) and (V-T) collisional exchange processes. The sole exception concerns V-T exchanges in N_2-N and H_2-H collisions for which multiquantum transitions are known to be important. For hydrogen there exists an efficient vibrational excitation mechanism (especially for upper vibrational levels $v > 3$) through electron impact excitation of the $H_2(B^1\Sigma_u^+)$ and $H_2(C^1\Pi_u)$ states followed by fast decay to excited vibrational levels of the electronic ground state $H_2(X^1\Sigma_g^+, v)$ [6]. A detailed list of processes and corresponding rate coefficients is given in [6]–[11], [14], [16]. A large number of collisional-radiative processes involving electronically excited states of N_2 and H_2 molecules and Ar atoms was taken into consideration in the models developed. A list of the major processes with the corresponding rate coefficient was given in recent works [9], [10], [14].

B. Charged Particle Balance and Maintaining Field

For the self-consistent determination of the electric field maintaining the discharge a balance between the rates of charged particles production and loss has to be obeyed. For example, in order to determine the electric field $E(z) = \sqrt{E_r^2(z) + E_z^2(z)}$ maintaining a steady-state N_2–Ar discharge the continuity equations for electrons and positive ions $[N_2^+, N_4^+, Ar^+, Ar_2^+]$ together with the quasineutrality condition $[n_e = N_2^+ + N_4^+ + Ar^+ + Ar_2^+]$ are solved consistently. In fact, the field strength necessary for the steady-state discharge operation is obtained from the balance between the total rate of ionization including direct, associative ionization [between the metastables $N_2(A^3\Sigma_u^+)$ and $N_2(a'^1\Sigma_u^-)$], pooling ionization [involving $Ar(^1P_1, ^3P_0, ^3P_1, ^3P_2)$] and step-wise ionization processes [from $N_2(A^3\Sigma_u^+, a'^1\Sigma_u^-, B^3\Pi_g)$] and the total rate of electronic losses due to diffusion to the wall and electron–ion bulk recombination (see Table I; here the symbol $f(E/N)$ is used to note that the electron rate coefficients for the corresponding processes are calculated from the electron Boltzmann equation. Data for recombination coefficients are taken from the literature as a function of the electron "temperature", i.e., $2/3$ of the electron mean energy for the present non-Maxwellian

TABLE I

Process	Rate constants (cm^3s^{-1})	Ref.
$e + N_2(X^1\Sigma_g^+, v = 0) \rightarrow N_2^+ + e + e$	$Z_1 = f(E/N)$	[16]
$e + N_2(A^3\Sigma_u^+) \rightarrow N_2^+ + e + e$	$Z_2 = f(E/N)$	[17]
$e + N_2(a'^1\Sigma_u^-) \rightarrow N_2^+ + e + e$	$Z_3 = f(E/N)$	[18]
$e + N_2(B^3\Pi_g) \rightarrow N_2^+ + e + e$	$Z_4 = f(E/N)$	[19]
$e + Ar \rightarrow Ar^+ + e + e$	$Z_5 = f(E/N)$	[20]
$N_2(A^3\Sigma_u^+) + N_2(a'^1\Sigma_u^-) \rightarrow N_4^+ + e$	0.9×10^{-11}	[21]
$N_2(A^3\Sigma_u^+) + N_2(a'^1\Sigma_u^-) \rightarrow N_2(X^1\Sigma_g^+, v = 0) + N_2^+ + e$	0.1×10^{-11}	[21]
$N_2(a'^1\Sigma_u^-) + N_2(a'^1\Sigma_u^-) \rightarrow N_4^+ + e$	$0.9 \times 5 \times 10^{-11}$	[21]
$N_2(a'^1\Sigma_u^-) + N_2(a'^1\Sigma_u^-) \rightarrow N_2(X^1\Sigma_g^+, v = 0) + N_2^+ + e$	$0.1 \times 5 \times 10^{-11}$	[21]
$e + N_2^+ \rightarrow N(^4S) + N(^4S)$	$\alpha_{r1} = 4.8\times10^{-7}\left(\frac{300}{T_e(K)}\right)^{1/2}$	[22]
$e + N_4^+ \rightarrow N_2(X^1\Sigma_g^+, v = 0) + N_2(X^1\Sigma_g^+, v = 0)$	$\alpha_{r2} = 2\times10^{-6}\left(\frac{300}{T_e(K)}\right)^{1/2}$	[22]
$e + Ar_2^+ \rightarrow Ar^* + Ar$	$\alpha_{r3} = 5.06\times10^{-9}(T_e(eV))^{-0.67}$	[23,24]
$Ar(s_j) + Ar(s_i) \rightarrow Ar(^1S_0) + Ar^+ + e$	$k_p = 3{,}69\times10^{-11}\sqrt{T_g}$	[24]

EEDF's). Taking into consideration the processes mentioned above, the electron continuity equation reads:

$$\begin{aligned} &n_e N_2 Z_1 + n_e N_2(A) Z_2 + n_e N_2(a') Z_3 + n_e N_2(B) Z_4 \\ &\quad + n_e Ar Z_5 + k_p \sum_{j=1}^{4} \sum_{i=1}^{j} Ar(s_i) Ar(s_j) \\ &\quad + N_2(a) N_2(A) Z_{\text{ass1}} + N_2(a')^2 Z_{\text{ass2}} \\ &\qquad = n_e \frac{D_{\text{ae}}}{\Lambda_{\text{eff}}^2} + \alpha_{r1} n_e [N_2^+] + \alpha_{r2} n_e [N_4^+] + \alpha_{r3} n_e [Ar_2^+] \end{aligned} \tag{1}$$

where A, a′, B denote the states $N_2(A^3\Sigma_u^+, a'^1\Sigma_u^-, B^3\Pi_g)$, respectively, D_{ae} is an ambipolar diffusion coefficient for electrons in the presence of several types of ions and Λ_{eff} is an effective diffusion length (which is determined assuming that all types of ions reach the corresponding ion sound speed at the plasma-sheath boundary) [14]. The expressions for the ambipolar diffusion coefficients of the different types of ions and for the electrons are given in [1], [14]. Note that the electron continuity (1) is strongly nonlinear in E due to the strong dependence of the electron rate coefficients on the electric field. Small changes in the field result in large changes in the high-energy part of the EEDF, and thus in the electron rate coefficients for excitation and ionization.

C. Gas and Wall Heating

The gas and wall temperatures influence strongly the rate coefficients for numerous bulk and surface reactions. Thus, their values must be incorporated self-consistently into the models. Under nearly isobaric conditions, neglecting the axial transport of the particles and assuming a parabolic gas temperature radial profile in agreement with experimental evidence [25], the stationary gas thermal balance equation can be written in the form [6]:

$$\frac{8\lambda(T_g)}{R^2}(T_g - T_w) = Q_{\text{in}} \tag{2}$$

Here, T_g is the radially averaged gas temperature, T_w is the wall temperature and $\lambda(T_g)$ is the gas thermal conduction. Thermal conduction to the tube wall usually is the main gas cooling mechanism. The wall temperature is introduced as an input parameter, either determined experimentally [8], [9] or by semi-empirical formulas [10], [15]. It was found that the measured axial distribution of the wall temperature for the hydrogen discharge can be well fitted by the semi-empirical formula [15]

$$T_w = T_0 + C(WR)^\beta$$

Here, T_0 is the room temperature in K, W (in Watt/cm^3) is the specific discharge power, R is the tube radius in cm, and C and β are fitting parameters. The axial variations of the wall temperature in N_2–Ar mixtures is calculated by the formula

$$T_w(z) = Tw(z = z_o) - \text{const}(dP/dz)$$

as obtained by a fit to experimental data (Fig. 2) [11]. Here, the dependence on the wave power absorbed per unit discharge length (dP/dz) is introduced. The position of the wave launcher is at z_o.

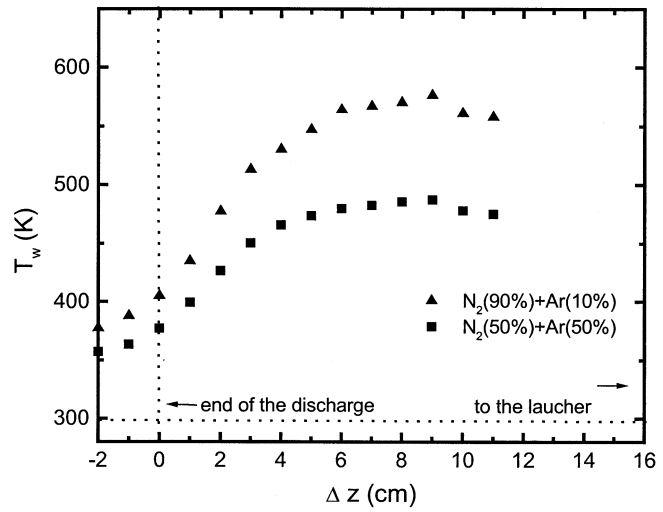

Fig. 2. Axial variation of the wall temperature in N_2–Ar discharge ($p = 2$ torr, $\omega/2\pi = 2.45$ GHz, $R = 0.7$ cm; Δz is the distance from the end of the discharge).

The right-hand-side of (2) $Q_{\rm in}$, accounts for the net power transferred per unit volume to the translational modes from volume and wall sources of heat. The bulk excitation processes of vibrational states of H_2 and N_2 followed by vibrational relaxation via N_2-N_2, N_2-N, N_2–Ar, H_2-H, H_2-H_2 collisions constitute important gas heating sources [9], [10], [15]. At the high degrees of ionization peculiar for discharges operating at microwave frequencies, exothermic pooling reactions between $N_2(A^3\Sigma_u^+)$ metastables should also be taken into account [9].

$$N_2(A^3\Sigma_u^+) + N_2(A^3\Sigma_u^+) \rightarrow N_2(X^1\Sigma_g^+, v) + N_2(C^3\Pi_u) + \Delta E$$
$$N_2(A^3\Sigma_u^+) + N_2(A^3\Sigma_u^+) \rightarrow N_2(X^1\Sigma_g^+, v) + N_2(B^3\Pi_g) + \Delta E$$

Moreover, ion acceleration in the sheath with consequent generation of "hot" neutrals, gas phase species interactions with the surface (such as de-excitation of metastable particles and vibrationally excited states of molecules on the wall) and wall reassociation of atoms also contribute significantly to the total gas heating.

D. Wave Power Transfer

The theoretical treatment of the wave-to-plasma power transfer is based on a simultaneous solution of the wave and the electron power balance equations [8]–[10]. Consider a plasma slice of thickness Δ_Z at the axial position z. The amount of wave power locally absorbed by this plasma slice is $\Delta P = \theta(z) S n_e(z) \Delta z$, ($S$ denoting the plasma cross-section and θ is the mean power needed to maintain an electron–ion pair [8], [9]). Under steady-state conditions, the spatial rate of wave power change dP/dz is equal to the power absorbed by the electrons per unit discharge length. The local power balance equation is therefore

$$\theta(z) S n_e(z) = -\frac{dP}{dz} = 2\alpha(z) P(z_0) \exp\left(-\int_{z_0}^{z} 2\alpha(x)\, dx\right) \quad (3)$$

By differentiating (3), the following equation is readily obtained for the axial gradient of the electron density:

$$\frac{dn_e}{dz} = -\frac{2\alpha n_e}{1 - \frac{n_e}{\alpha}\frac{d\alpha}{dn_e} + \frac{n_e}{\theta}\frac{d\theta}{dn_e}} \quad (4)$$

This ordinary differential equation, stemming from basic electrodynamical relations, correlates in a self-consistent way the axial variation of the wave characteristics and the discharge parameters. Under the assumption of a slow variation of the plasma permittivity along the wave path, "local" field equations with a local dispersion relation are used in order to describe the discharge electrodynamics. The wave dispersion properties, i.e., the attenuation coefficient α and wave number β are derived as usual by considering the equations expressing the continuity of the field tangential components across the plasma-glass and glass-air interfaces (for details see for example [26] and references therein). This yields a set of homogeneous equations, with respect to the electric field components. The corresponding determinant must vanish in order that a nontrivial solution exists. The latter relation provides a local wave dispersion equation (LDE), which can symbolically be expressed as [26]:

$$D\lfloor \omega/\omega_{\rm pl}(z), \omega R/c, v_{\rm eff}(z)/\omega, \varepsilon_d, \mathrm{k} = \alpha + j\beta \rfloor = 0, \quad (5)$$

where $\omega_{\rm pl}(z) = (n_{\rm eff}(z) e^2/m_e\varepsilon_o)^{1/2}$ (e, m_e are the electron charge and mass respectively, ε_o is the vacuum dielectric permittivity) and $n_{\rm eff}$ and $\nu_{\rm eff}$ are ω-dependent effective values of the electron density and total electron–neutral collision frequency [26]. The numerical calculations are made in complex algebra. The (5) is solved locally for any position z within the geometrical optics approach i.e., the plasma is assumed locally homogeneous in axial direction [26]. According to the experimental situation, solutions for constant ω and variable $v_{\rm eff}(z)$ and $n_{\rm eff}(z)$ along the wave path are searched. For each value of $\nu_{\rm eff}(z)/\omega$ the two real parameters $\alpha_{\nu_{\rm eff}/\omega}(z)$ and $\beta_{\nu_{\rm eff}/\omega}(z)$ vs $n_{\rm eff}(z)$ are obtained.

E. Method of Solution

An example of the flow-chart of the solution algorithm used in order to solve self-consistently the system of equations is depicted in Fig. 3. The input parameters of the model are the wave frequency $\omega/2\pi$, the tube inner and outer radii R and R_1, respectively, the pressure p, the electron density at the position of the SW launcher $n_e(z_0)$ (or the total power needed to sustain the discharge) and the initial value of the wall temperature $T_w(z_0)$ at the position of the launcher.

The procedure starts with arbitrary values of the electric field E_o maintaining the discharge, the vibrational T_v^0 (introduced as a measure of the degree of vibrational excitation [14]) and the gas (T_g^0) temperature. The electron Boltzmann equation is solved by iterations. In the calculations of the EEDF, the accuracy achieved in the electron power balance equation (obtained as a third moment of the electron Boltzmann equation and yielding the value of θ) is better than 10^{-5}. By using the rate coefficients for electron impact processes, the nonlinear set of equations for heavy particles and ions is solved by applying the Newton-Raphson method. By iterations, convergent solutions for the VDF and the vibrational temperature T_v are obtained for given value of the E field. The electric field is then

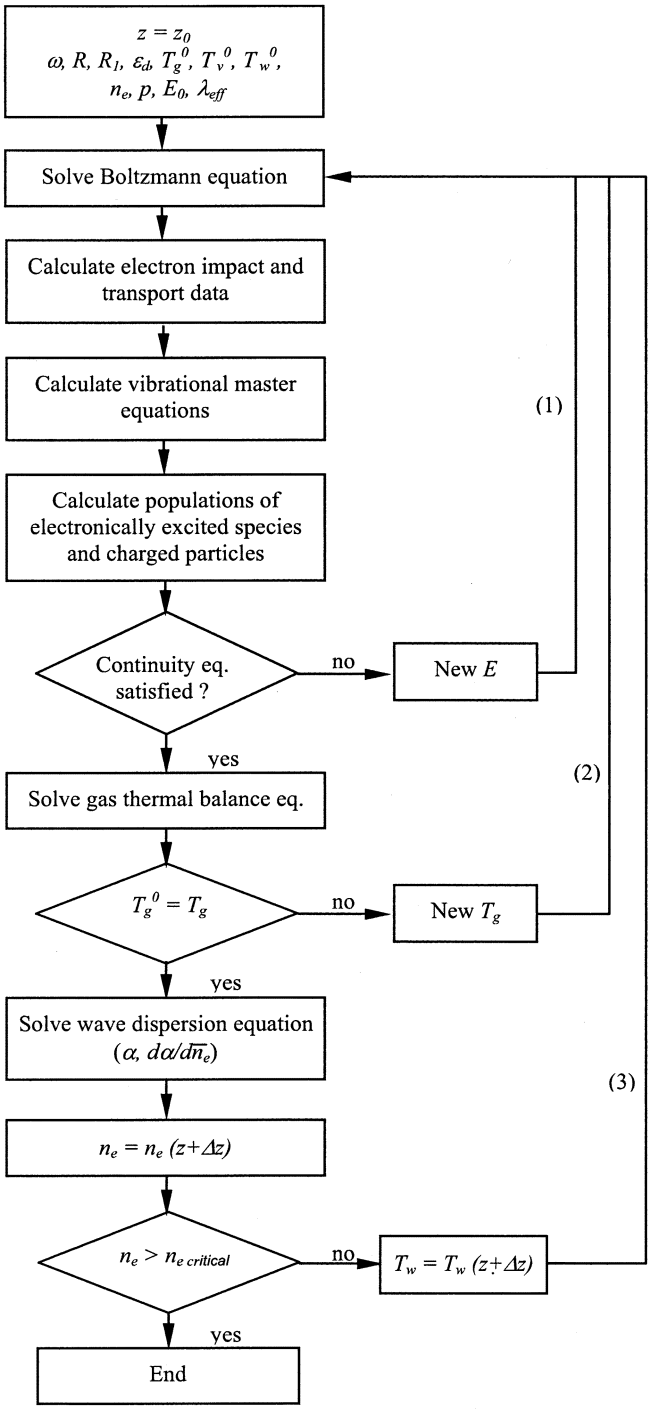

Fig. 3. Flow-chart of the model.

varied to satisfy the electron continuity (2). For the electric field determination, an accuracy better than 10^{-5} is achieved. As a result of this iterative loop, convergent solutions for the heavy particle density, the VDF and the electric field maintaining the discharge is achieved for a given value of the electron density $n_e(z)$. Then, the gas thermal balance (3) is solved and a new iteration procedure (loop 2) determines a self-consistent value of T_g. Using the self-consistently calculated values of $n_{\rm eff}(z)$ and $\nu_{\rm eff}(z)$ the local dispersion equation (LDE) is solved in complex algebra. The integration of (5) yields a new value of the electron density at the position $z+\Delta z$. Then a new value of the wall temperature is obtained from the semi-empirical formula used. The entire loop (3) is then repeated for the next axial position. So, point-by-point, the discharge and the wave characteristics are calculated along the plasma column until n_e reaches the critical value $n^{\rm cr}[\omega = (n_e e^2/m_e\varepsilon_0)^{1/2}]$, where it is assumed that the discharge stops.

The calculated results include the axial variation of the EEDF and its integrals, $\theta(z), n_e(z)$, the VDF of the electronic ground $N_2(X^1\Sigma_g^+, v)$ state δ_v, the population densities of the electronically excited states $N_2(A^3\Sigma_u^+, a'^1\Sigma_u^-, B^3\Pi_g, C^3\Pi_u, a^1\Pi_g, w^1\Delta_u)$, $Ar(^1P_1, ^3P_0, ^3P_1, ^3P_2)$, positive ions $(N_2^+, N_4^+, Ar^+, Ar_2^+)$ and nitrogen atoms in the ground state $N(^4S)$, electric field E, gas temperature T_g, and wave attenuation coefficient α and wave number β.

III. Dissociation Kinetics in H_2, N_2, and N_2–Ar Discharges

A. Molecular Dissociation in H_2 Surface Wave Sustained Discharge

In a pure hydrogen discharge, the H(1s) atom density is determined by the mechanisms listed in Table II. Dissociation of H_2 molecules with formation of two hydrogen atoms in the ground state H(1s) results mainly from direct excitation of the repulsive state $H_2(b^3\Sigma_u^+)$ by electron impact of intermediate and high-energy electrons on H_2 molecules as well as from the excitation of bound triplet states $H_2(c^3\Pi_u, a^3\Sigma_g^+, e^3\Sigma_u^+)$ followed by fast radiative decay into the $H_2(b^3\Sigma_u^+)$ state. Therefore, the sum of the rate coefficients for the excitation of these states appears as a rate coefficient for the dissociation of H_2 by electrons. Dissociation by electron impact yielding $H(1s) + H(n = 2)$ and $H(1s) + H(n = 3)$ are further considered. Dissociative attachment of slow electrons to vibrationally excited H_2 molecules and mutual neutralization of electrons and negative ions H^- with positive ions are also sources of ground state hydrogen atoms.

The ground state atoms are mainly destroyed through heterogeneous reactions on the wall. Such interactions are taken into account in a one-dimensional bulk model by using radially-averaged rates of wall losses ν_w (in s^{-1}) expressed in the form

$$\nu_w \approx \left(\frac{R^2}{5.8D} + \frac{2R}{\gamma\langle v\rangle}\right)^{-1}$$

where D is the diffusion coefficient, $\langle v\rangle$ is the particle mean velocity close to wall and γ is the probability of wall deactivation, i.e., the fraction of wall collisions leading to losses of the species. A pyrex wall is considered. The loss of H atoms at low-pressure conditions is mainly controlled by wall reassociation, due to their fast diffusion to the wall and the small value of γ. Thus the diffusion term can be ignored in determining the total wall loss rate. According to the results in [7] the following wall temperature dependence has been used for γ_H:

$$\gamma_H = \gamma_o \exp\left\{-\frac{840}{T_w}\right\} \tag{6}$$

where $\gamma_o = 1.2 \times 10^{-2}$ or $\gamma_o = 6 \times 10^{-2}$. These two values of γ_o and the wall temperature dependence (6) describe rather

TABLE II
KINETICS OF THE GROUND H(1s) STATE ATOMS IN HYDROGEN DISCHARGE

Process	Rate Coefficient (cm^3s^{-1})	Reference
$e + H_2(X^1\Sigma_g^+, v = 0) \rightarrow$ $e + H_2(b^3\Sigma_u^+, a^3\Sigma_g^+, c^3\Pi_u, e^3\Sigma_u^+) \rightarrow e + 2H_2(1s)$	*f(E/N)*	[27]
$e + H_2(X^1\Sigma_g^+, v = 0) \rightarrow e + H(1s) + H(n = 2)$	*f(E/N)*	[28]
$e + H_2(X^1\Sigma_g^+, v = 0) \rightarrow e + H(1s) + H(n = 3)$	*f(E/N)*	[28]
$H(1s) + wall \xrightarrow{\gamma_H} \frac{1}{2} H_2(X^1\Sigma_g^+, v = 0) + wall$		[7]
$e + H_2^+ \rightarrow H(1s) + H(1s)$	3×10^{-8} $(300/T_e)^{0.5}$	[29]
$e + H_3^+ \rightarrow H_2 + H(1s)$	1.55×10^{-8} $(300/T_g)^{0.97}$	[30]
$H^- + H(1s) \rightarrow H_2(X^1\Sigma_g^+, v = 0) + e$	1.8×10^{-9}	[31]
$H^- + H_2^+ \rightarrow 3H(1s)$	2×10^{-7} $(300/T_g)$	[6]
$H^- + H_3^+ \rightarrow H_2 + 2H(1s)$	2×10^{-7} $(300/T_g)$	[6]

well different experimental measurements which can be split into two data sets. The difference in approximately a factor of 5 between the values of γ_H for these two sets can be connected with different technologies for the production of Pyrex glass: i) large difference in the roughness factors; ii) large differences in the surface densities of chemically active sites, which control the value of γ_H. This could be connected, for example, with different surface densities of admixtures, defects, partial occupation of active sites by chemically nonactive molecules, etc.

Wall reassociation is usually associated with chemisorbed atoms, i.e., irreversibly adsorbed atoms at active sites on the wall. The surface is covered with a small fraction of such active sites. Chemisorbed atoms can recombine with atoms arriving at the active sites either directly from the gas phase (Eley-Rideal mechanism) or from physisorbed (reversibly adsorbed) atoms, by diffusion along the surface (Langmuir-Hinshelwood mechanism) [32]. The losses of gas phase atoms on a Pyrex surface in the range of wall temperatures $T_w < 500$ K may be attributed to the Langmuir-Hinshelwood mechanism [7], [15]. This fact can be recognized on Fig. 4 where the dependence of the degree of dissociation on the wall temperature is depicted. An externally forced "local" (at a fixed axial pozition $\Delta z/L_t = 0.17$ in respect to the plasma column end, $L_t = 18$ cm) cooling/heating of the tube wall of a surface wave sustained discharge operating at 500 MHz has been performed. Clearly, the number density of H(1s) atoms decreases when T_w locally increases up to about 400 K, thus following the wall temperature dependence of the wall reassociation probability (6).

The dissociation degree of hydrogen molecules K_d was determined by applying an emission spectroscopy method based on the measurement of the ratio of the H_α line intensity $I_{H\alpha}$ of atomic hydrogen to the integrated intensity of the Fulcher α band system emission ($d^3\Pi_u^-, v' \rightarrow a^3\Sigma_g^+, v''$) ($Q$ branch) of molecular hydrogen I_{H_2} (see Fig. 5) [33]–[35]

$$\frac{I_{H_\alpha}}{I_{H_2}} = \frac{\langle \sigma_{H_\alpha}^{\text{diss}} V_e \rangle}{\langle \sigma_{H_2} V_e \rangle} + \frac{2K_d}{1 - K_d} \frac{\langle \sigma_{H_\alpha} V_e \rangle}{\langle \sigma_{H_2} V_e \rangle}. \tag{7}$$

Here $\langle \sigma_{H_2} V_e \rangle, \langle \sigma_{H_\alpha}^{\text{diss}} V_e \rangle, \langle \sigma_{H_\alpha} V_e \rangle$ are the rate constants (averaged over the electron energy distribution under assumption, in this case, of Maxwellian electron energy distribution function

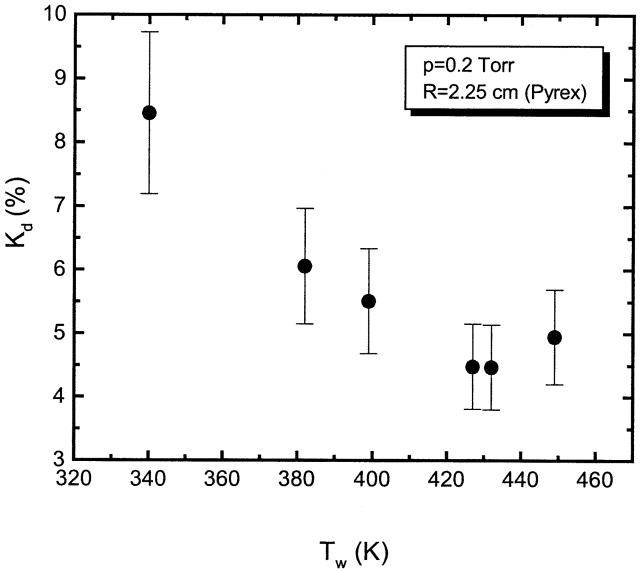

Fig. 4. Wall temperature dependence of the degree of hydrogen dissociation.

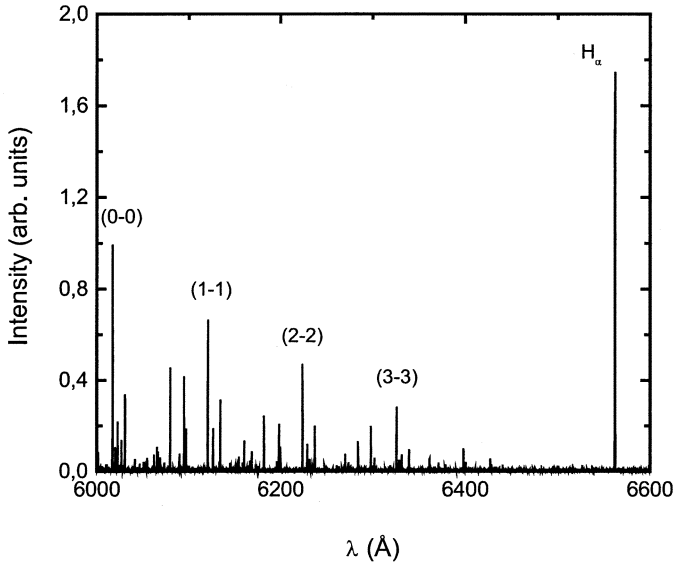

Fig. 5. Emission spectrum of an hydrogen surface wave sustained discharge ($p = 0.15$ torr, $\omega/2\pi = 500$ MHz, $R = 2.25$ cm, Pyrex tube).

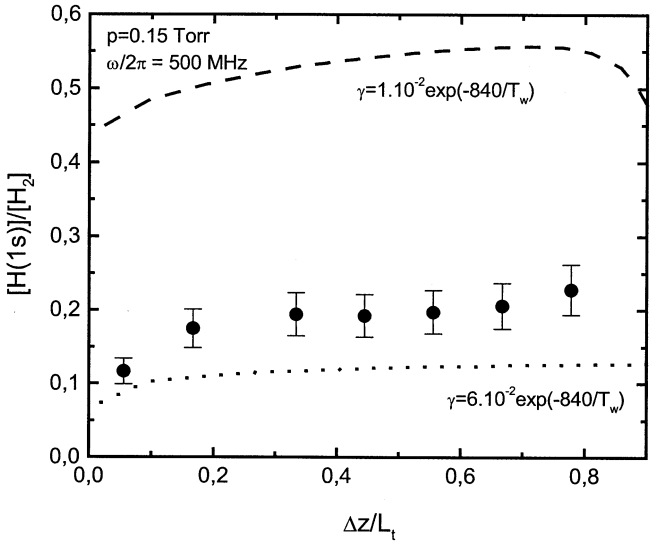

Fig. 6. Axial variation of the hydrogen atom relative number.

of free plasma electrons) for excitation of $H_2(d^3\Pi_u^-)$ level, dissociative and direct excitation of the H_α line, respectively, and V_e is the electron thermal velocity. Data for cross sections, transition probabilities and radiative lifetimes are taken from [34]. Conventional probe diagnostic techniques described elsewhere have been applied in order to obtain the electron temperature T_e.

The experimental results for the axial variation of the relative H(1s) number density along the plasma column and the model predictions for two scaling values of γ_o are shown in Fig. 6. The axial position is normalized to the total discharge length, L_T, in such a way that $\Delta z/L_T = 1$ corresponds to the position of the launcher and $\Delta z/L_T = 0$ to the plasma column end. Due to the strong dependence of the wall reassociation probability on the wall temperature (which decreases toward the end) the H(1s) density could be expected to increase toward the plasma column end. However, the decrease in electron density reduces the rate of dissociation, and the relative number of hydrogen atoms falls close to the end. The theoretical results are in closer agreement with the experimental ones when a higher reassociation probability is assumed. As seen, there is drastic dependence of the degree of molecular dissociation on the wall conditions. Depending on the wall reassociation probability the relative atom density [H(1s)]/[H_2] can vary significantly [15]. Thus the obtained results suggest that the external change of the wall temperature can be used to achieve dynamic control of the molecular dissociation in hydrogen discharges.

B. Molecular Dissociation in N_2 Surface Wave Sustained Discharge

The main source channel of ground state N(^{4}S) nitrogen atoms in a microwave discharge at low pressure conditions is electron impact dissociation according to the reactions

$$e + \mathrm{N_2}(\mathrm{X}^1\Sigma_g^+, v = 0) \rightarrow e + \mathrm{N}(^4\mathrm{S}) + \mathrm{N}(^4\mathrm{S})$$
$$e + \mathrm{N_2}(\mathrm{X}^1\Sigma_g^+, v = 0) \rightarrow e + \mathrm{N}(^4\mathrm{S}) + \mathrm{N}(^2\mathrm{D}).$$

Dissociative recombination between electrons and N_2^+ ions constitutes another source channel

$$e + \mathrm{N_2^+} \rightarrow e + \mathrm{N}(^4\mathrm{S}) + \mathrm{N}(^4\mathrm{S}).$$

Atomic re-association on the wall is one of the loss channels of N(^{4}S) ground state atoms:

$$\mathrm{N}(^4\mathrm{S}) + \mathrm{wall} \xrightarrow{\xi} \frac{1}{2}\mathrm{N_2}(\mathrm{X}^1\Sigma_g^+, v = 0).$$

Here, ξ is the probability of wall re-association whose value depends on the surface conditions [32].

Other loss channels for ground state atoms are electron impact excitation to atomic metastable states

$$e + \mathrm{N}(^4\mathrm{S}) \rightarrow e + \mathrm{N}(^2\mathrm{D}, ^2\mathrm{P})$$

and quenching by metastable $N_2(A^3\Sigma_u^+)$ molecules

$$\mathrm{N_2}(\mathrm{A}^3\Sigma_u^+) + \mathrm{N}(^4\mathrm{S}) \rightarrow \mathrm{N_2}(\mathrm{X}^1\Sigma_g^+, 6 \leq v \leq 9) + \mathrm{N}(^2\mathrm{P}).$$

These reactions do not correspond to complete loss of ground state atoms because the metastable atoms N(^{2}D,^{2}P) so formed are partly converted back to the ground state N(^{4}S) by electron superelastic collisions, destruction at the wall and quenching by N_2 molecules (see Table III). Therefore, the volume kinetics of atoms excited in metastable states and their interactions with the wall have a significant influence on the dissociation processes in a nitrogen discharge. The kinetics of N(^{2}D,^{2}P) metastable states is taken into account by considering the source and the loss channels listed in Table III. When metastable atoms diffuse to the wall they are destroyed by quenching or reassociation into N_2 molecules. In the present model, we assume that a certain fraction ζ of metastable atoms arriving at the wall are quenched to ground state N(^{4}S), while the remaining fraction $1 - \zeta$ recombine into N_2 molecules. In order to demonstrate the sensitivity of the results to this parameter, the axial variation of the relative concentration of ground state atoms for two

TABLE III
KINETICS OF THE N(^{2}D) AND N(^{2}P) ATOMIC METASTABLE STATES IN A NITROGEN DISCHARGE

	Process	Rate Coefficient (cm^3s^{-1})	Reference
R1	$e+N_2 \rightarrow e+N(^4S)+N(^2D)$	*f(E/N)*	[21]
R2	$e+N(^4S) \leftrightarrow e+N(^2D)$	*f(E/N)*	[36]
R3	$e+N(^4S) \leftrightarrow e+N(^2P)$	*f(E/N)*	[36]
R4	$e+N(^2D) \leftrightarrow e+N(^2P)$	*f(E/N)*	[36]
R5	$N(^2D)+N_2 \rightarrow N(^4S)+N_2$	$10^{-13}\exp(-510/T_g)$	[37]
R6	$N(^2D)+N(^2P) \rightarrow N_2^+ + e$	10^{-13}	[38]
R7	$N_2(A)+N(^4S) \rightarrow N_2(X,6\leq v\leq 9)+N(^2P)$	4×10^{-11}	[21]
R8	$N(^4S)+N(^2P) \rightarrow N(^4S)+N(^2D)$	6×10^{-13}	[38]
R9	$N(^4S)+N(^2P) \rightarrow N(^4S)+N(^4S)$	1.8×10^{-12}	[38]
R10	$N(^2P)+N_2 \rightarrow N(^4S)+N_2$	6×10^{-14}	[38]
R11	$N(^2P)+N_2(X^1\Sigma^+_g,v\geq10) \rightarrow N(^4S)+N_2(A)$	$10^{-10}\exp(-1300/T_g)$	[38]
R12	Diffusion of N(^{2}D) to the wall	$ND=6.4\times10^{18}(T_g/300)^{0.5}$	[39]
R13	Diffusion of N(^{2}P) to the wall	$ND=5.2\times10^{18}(T_g/300)^{0.5}$	[39]

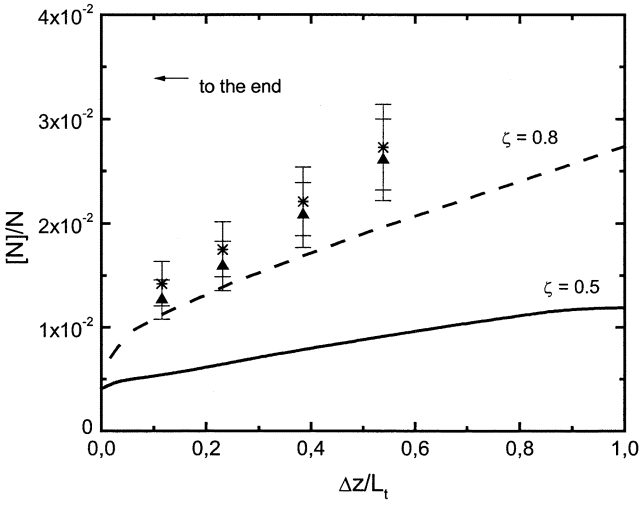

Fig. 7. Relative concentration of N(^{4}S): experimental measurements $(*, \Delta)$; $(---, —)$ calculations (N_2 discharge, $p = 2$ torr, $\omega/2\pi = 2.45$ GHz, $R = 0.7$ cm).

different values of ζ is shown in Fig. 7. As can be seen, the relative concentration of ground state atoms decreases toward the column end, essentially as a consequence of the decrease in the electron density along the discharge. The experimental results, also shown in the figure, are close to the theoretical ones when the $\zeta = 0.8$ is assumed, i.e., most metastable atoms reaching the wall are converted back to the ground state.

The atomic concentration has been measured by applying an actinometry technique [40] using Ar as actinometer. The experiments are performed in a nitrogen microwave discharge operating at the frequency $\omega/2\pi = 2.45$ GHz and pressure $p = 2$ torr. Intense nitrogen atomic lines belonging to the transition $(3p^4S^0 \rightarrow 3s^4P)$ have been detected in the emission spectrum of the discharge as seen from Fig. 8. The intensity ratios of the two nitrogen atomic lines $\lambda = 744.23$ nm and $\lambda = 746.83$ nm to the $\lambda = 750.39$ nm argon atomic line (transition $2p_1 \rightarrow 1s_2$) have been detected as a measure of the relative concentration of

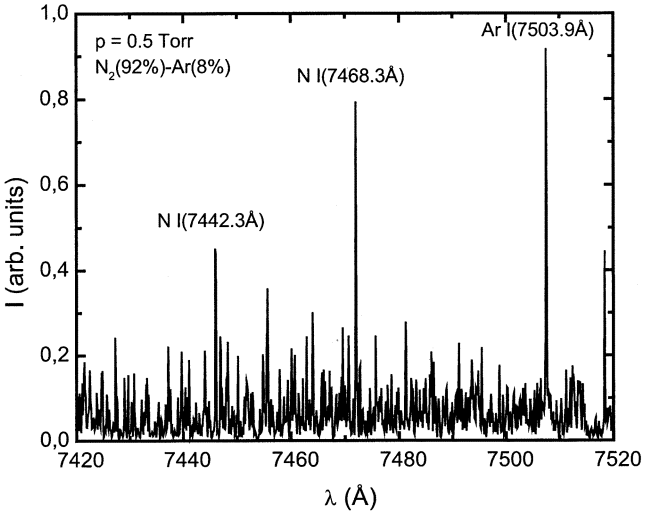

Fig. 8. Emission spectrum of the N_2 discharge.

ground state nitrogen atoms [N(^{4}S)]/[N_2]. In order to determine the concentration of N(^{4}S) atoms it has been assumed that the $N(3p^4S^0)$ and $Ar(2p_1)$ excited states are principally populated by direct electron impact excitation of the atomic ground state and lost by radiative de-excitation or quenching by nitrogen molecules and argon atoms.

The relative concentration of ground state N(^{4}S) atoms can be calculated using the relation [11]:

$$\frac{[N(^4S)]}{[N_2]} = \frac{R_{(750)}}{R_{(744)}}\frac{h\nu_{(750)}}{h\nu_{(744)}}\frac{A_{750}}{A_{744}}\frac{k_{Ar}}{k_N} \times \frac{\left\{\sum A^N_{ij} + K^N_{N_2}[N_2] + K^N_{Ar}[Ar]\right\}}{\left\{\sum A^{Ar}_{ij} + K^{Ar}_{N_2}[N_2] + K^{Ar}_{Ar}[Ar]\right\}}\frac{[Ar]}{[N_2]}\frac{I(744)}{I(750)}. \quad (8)$$

Here, $\sum_j A^N_{ij}, \sum_j A^{Ar}_{ij}$ are the emission probabilities for all the radiative de-excitation processes from the considered excited levels ($A_{744} = 1.06 \times 10^7$ s^{-1} and $A_{750} = 4.72 \times 10^7$ s^{-1}), $R_{(744)}$ and $R_{(750)}$ represent the spectral response of the system at 744 and 750 nm respectively, $K^N_{N_2} = 3.8 \times 10^{-10}$ cm^{3}s^{-1} and $K^N_{Ar} = 3.8 \times 10^{-10}$ cm^{3}s^{-1} are the quenching coefficients of the $N(3p^4S^0)$ state by Ar atoms and N_2 molecules. The mean values $K^{Ar}_{N_2} = 3.2 \times 10^{-11}$ cm^{3}s^{-1} and $K^{Ar}_{Ar} = 1.6 \times 10^{-11}$ cm^{3}s^{-1} are taken for the quenching coefficients of excited Ar atoms [11], [40]. [N_2] is the total nitrogen concentration. The total nitrogen and argon concentrations and the ratio [Ar]/[N_2] can be calculated from the measured gas temperatures (under nearly isobaric conditions, by applying the ideal gas law $p = NkT_g$) and the flow rates of the gas components [8], [11]. The variations of the ratio k_{Ar}/k_N are accounted for by using the experimentally obtained electron temperatures.

Fig. 9 shows the contribution of the different destruction channels of N(^{4}S) atoms: recombination at the wall (full curve): electron impact destruction by the reaction $e + N(^4S) \rightarrow e + N(^2D)$ (broken curve) (R2 in Table III); electron impact destruction by reaction $e + N(^4S) \rightarrow e + N(^2P)$ (dotted curve) (R3); and destruction in collisions with the metastable state $N_2(A^3\Sigma^+_u)$ through reaction $N_2(A) + N(^4S) \rightarrow N_2(X, 6 \leq v \leq 9) + N(^2P)$ (R7, chain curve). Close to the launcher, where the electron density is higher, the destruction processes by electron impact dominate.

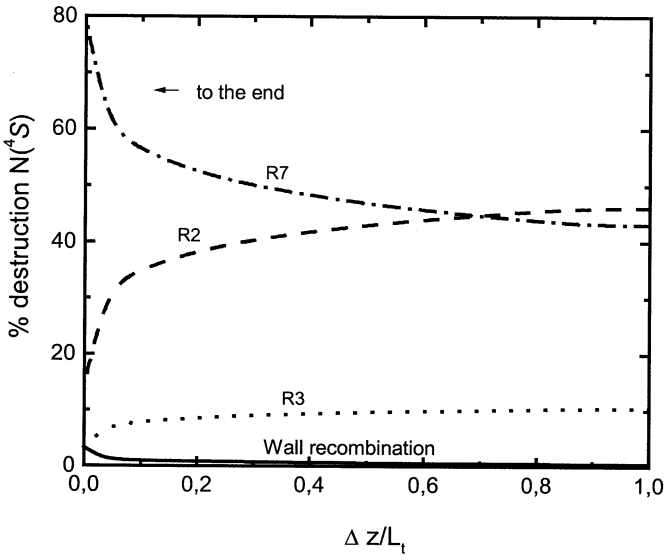

Fig. 9. Percentage contributions of the various destruction processes of N(^{4}S) atoms along the discharge length: N(^{4}S) + wall $\rightarrow$ (1/2)N_2(X, v = 0)(—); reaction R2 (– – –); R3 (· · ·); R7 (– · –).

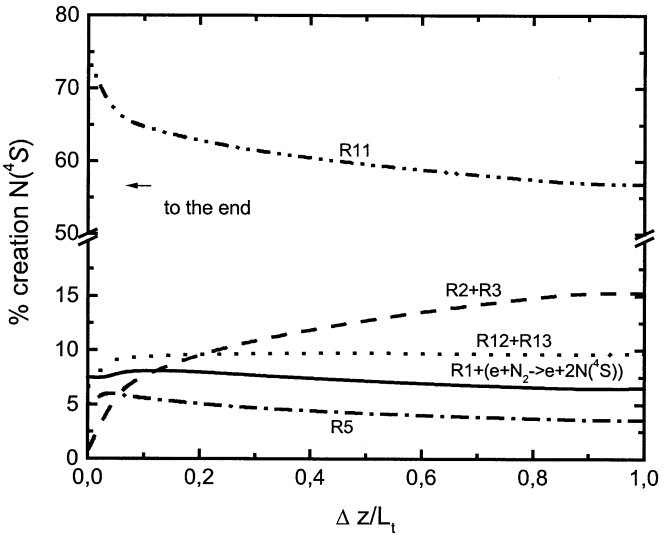

Fig. 10. Percentage contributions of the various creation processes of N(^{4}S) atoms along the discharge length: dissociation of N_2 by electron impact, e + N_2 $\rightarrow$ N(^{4}S) + N(^{4}S) and e + N_2 $\rightarrow$ N(^{4}S) + N(^{2}D)(—); reaction R2 and R3 (– – –); R12 and R13 (· · ·); R5 (– · –); R11 (··).

However, as one moves along the discharge axis toward the plasma column end, the reaction with $N_2(A^3\Sigma_u^+)$ metastables starts to dominate. Destruction of ground state atoms at the wall seems to be a minor loss channel. Nevertheless, there exists large uncertainties in the collisional data in particular in the value of the recombination probability of nitrogen atoms at the wall. Here, we consider $\gamma_N = 5 \times 10^{-4}$ [9], [32]. A larger value of γ_N would lead to a higher contribution of wall losses. It should be emphasized that reactions R2, R3, and R7 do not destroy effectively ground state N(^{4}S) atoms because most atoms excited in metastable states trough these reactions subsequently give back N(^{4}S). This can be seen in Fig. 10 where the percentage contribution of the different source channels of N(^{4}S) atoms is presented: electron impact dissociation of N_2 (full curve); electron superelastic collisions with metastable atoms e+N(^{2}D, ^{2}P) $\rightarrow$ e+N(^{4}S) (R2, R3 broken curve); deactivation of metastable atoms at the wall N(^{2}D, ^{2}P) + wall $\rightarrow$ N(^{4}S) (R12 and R13 dotted curve); quenching of N(^{2}D) by N_2 molecules N(^{2}D) + N_2 $\rightarrow$ N(^{4}S) + N_2 (R5 chain curve); quenching of N(^{2}P) by vibrationally excited molecules N(^{2}P) + $N_2(X^1\Sigma_g^+ v \geq 10)$ $\rightarrow$ N(^{4}S) + N_2(A) (R11 double chain curve). Other processes not shown here have negligible contribution for the conditions considered. The calculations show that approximately 90% of the created metastable atoms give back N(^{4}S). Furthermore R7 is the main reaction for N(^{4}S) destruction but it is practically cancelled by the reverse reaction R11 which constitutes the main source of ground state atoms. Thus, these two reactions ensure a strong correlation between the atom kinetics and that of the $N_2(A^3\Sigma_u^+)$ metastable. In this way, the detailed kinetics of metastable atoms and $N_2(A^3\Sigma_u^+)$ molecules is essential to determine the concentration of ground state atoms as the results demonstrate.

C. Molecular Dissociation in N_2–Ar Discharge

At the high degrees of ionization of the present situation, the production of N(^{4}S) by dissociative recombination e + N_2^+ $\rightarrow$ N(^{4}S) + N(^{4}S) plays a significant role and provides an increase in the dissociation degree of N_2 molecules in N_2–Ar discharge. This is related to the fact that N_2^+ ions are the dominant positive ions even at high Ar fractional percentages in the mixture (Fig. 11). In addition to a number of source channels contributing to N_2^+ creation in a pure N_2 discharge (see Table I), i.e., electron impact ionization, associative ionization and step-wise ionization, fast charge transfer processes

$$Ar^+ + N_2 \leftrightarrow N_2^+ + Ar$$

contribute also to N_2^+ production in N_2–Ar mixture. It should be emphasized the charge transfer rate increases with vibrational excitation. Here, the mean values 4.45×10^{-10} cm^{3}s^{-1} and 2.81×10^{-10} cm^{3}s^{-1} have been used for the corresponding processes [41]. The relative contribution of the different source

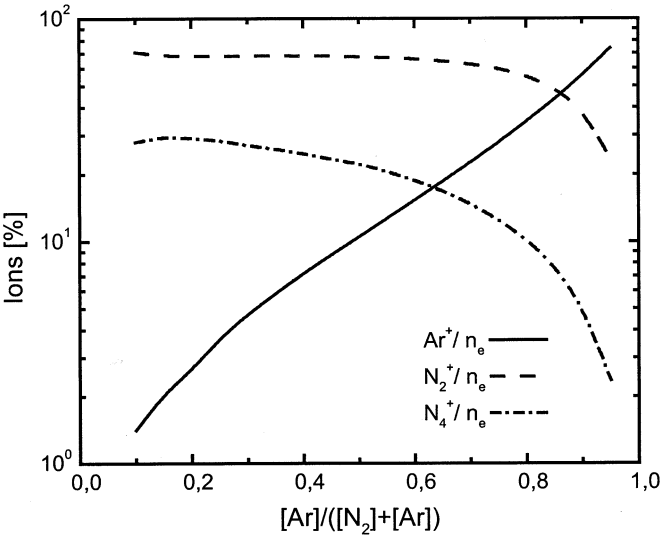

Fig. 11. Percentage variation of the positive ion density in N_2–Ar discharge as a function of the mixture composition (p = 2 torr, $\omega/2\pi$ = 2.45 GHz, R = 0.7 cm; $n_e = 1.2 \times 10^{18}$ m^{-3} = const).

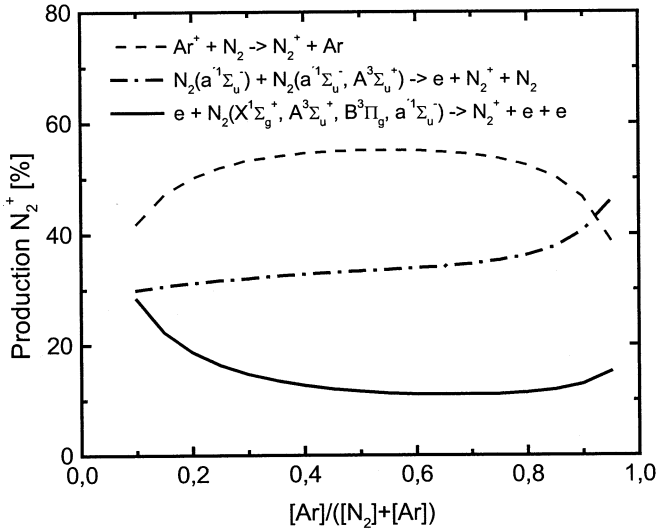

Fig. 12. Relative variation of N_2^+ ion source channels with Ar percentage ($p = 1$ torr, $n_e = 1.5 \times 10^{18}\ m^{-3} = \text{const}$).

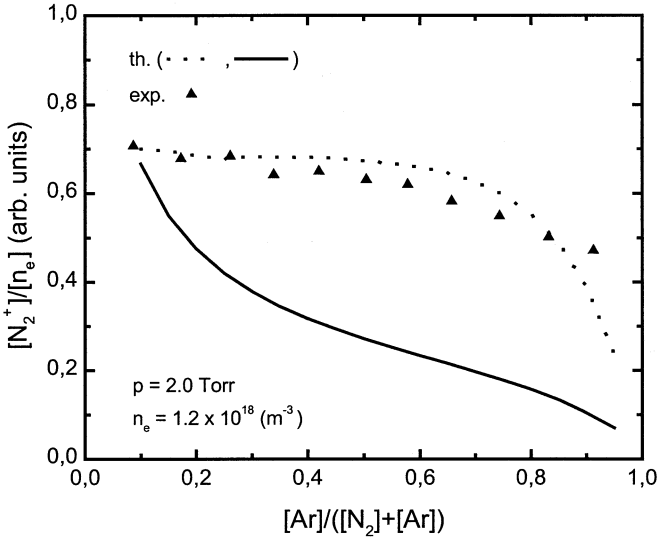

Fig. 13. Dependence of N_2^+ ion relative number on Ar percentage. The dashed and solid curves are theoretical calculations with and without charge exchange processes ($Ar^+ + N_2 \leftrightarrow Ar + N_2^+$) taken into account, respectively.

channels to the total N_2^+ production depends on the pressure and mixture composition (see Fig. 12). At lower pressure the contribution of the charge transfer $Ar^+ + N_2 \rightarrow N_2^+ + Ar$ is dominant while at higher pressures associative ionization prevails. Collisional quenching of $N_2(B^3\Pi_g, a'^1\Sigma_u^-, a^1\Pi_g)$ states with Ar atoms enhances the relative population in the $N_2(A^3\Sigma_u^+)$ state. The radiative and collisional coupling between $N_2(A^3\Sigma_u^+)$, $N_2(B^3\Pi_g)$ and $N_2(C^3\Pi_u)$ states is strongly influenced by the presence of Ar atoms in the N_2–Ar discharge due to the following chain of reactions [10], [11]:

$$N_2(a^1\Pi_g) + Ar \rightarrow N_2(a'^1\Sigma_u^-) + Ar \rightarrow N_2(B^3\Pi_g) + Ar \rightarrow N_2(A^3\Sigma_u^+) + Ar$$

Quenching of $N_2(a'^1\Sigma_u^-)$ and $N_2(a^1\Pi_g)$ in collisions with Ar atoms populates $N_2(B^3\Pi_g)$ and the subsequent quenching of this state in collisions with molecules (N_2) and atoms (Ar) along with radiative decay effectively populate $N_2(A^3\Sigma_u^+)$. As a result, the contribution of associative ionization through $N_2(A^3\Sigma_u^+)$ also increases.

The emission of the $N_2^+(B^2\Sigma_u, v = 0 \rightarrow X^2\Sigma_g, v = 0)$ 391.4 nm band is indicative of the N_2^+ presence in the discharge [8]. The $N_2^+(B^2\Sigma_u, v)$ state is excited from $N_2^+(X^2\Sigma_g, v)$ both by direct electron impact and by energy exchange reactions in collisions of $N_2^+(X^2\Sigma_g, v)$ ions with vibrationally excited $N_2(X^1\Sigma_g^+, v > 12)$ molecules. When the condition $\sum_{v>12}\lfloor N_2(X^1\Sigma_g^+, v)\rfloor \approx \text{const}$ is nearly fulfilled, one can assume that $\lfloor N_2^+\rfloor \propto I(N_2^+(B^2\Sigma_u, v' = 0 \rightarrow X^2\Sigma_g, v'' = 0))$. The variation of the 391.4-nm line intensity I(391) versus the Ar percentage in the mixture is shown in Fig. 13. The measurements are performed close to the launcher ($\Delta z/L_t \approx 1$) in a microwave surface wave sustained discharge operating at the frequency $\omega/2\pi = 2.45$ GHz in an N_2–Ar mixture ($R = 0.75$ cm) at constant pressure and nearly constant electron density. For the purposes of comparison, the predicted variation of the N_2^+ density as the Ar percentage changes (two different cases are considered) is also shown. As seen, discarding the contribution of the fast charge transfer processes $Ar^+ + N_2 \leftrightarrow N_2^+ + Ar$ (solid line in the Fig. 13) results in a different behavior of the N_2^+ density when the mixture composition is changed. The predicted behavior of the N_2^+ relative number density follows the experimental one only when the above charge transfer processes are taken into consideration (dashed line on the figure). These results are indicative of a significant contribution of charge exchange between N_2 and Ar^+ to the creation of N_2^+ at higher Ar percentages for the present conditions [11].

The variation of the relative density of ground state atoms versus the Ar percentage when the electron density and the pressure are kept constant is shown in Fig. 14. As seen, the change in Ar percentage in the mixture results in a peculiar behavior of the N_2 dissociation degree. The experimental (i.e., from relation 8) and the theoretical dependences (solid curves) of the N_2 dissociation on the Ar percentage show a good agreement assuming that 90%–95% of atoms in metastable states give back ground state N(^{4}S) atoms (due to the bulk and wall quenching). At low pressure ($p = 0.5$ torr, Fig. 14(a)) the N(^{4}S) relative density first drops but then increases as the Ar percentage grows. At higher pressure ($p = 2$ torr, Fig. 14) it remains approximately constant for Ar fractional percentages between 20% and 80%. The relative number density of the ground state atoms varies between 5 and 10% for the conditions considered. The competition between source channels, presented in Fig. 15, determines the dissociation degree dependence on the Ar percentage. At lower Ar percentage, electron impact dissociation has a dominant contribution to the production of ground state atoms, while for Ar fractional percentages higher than 50% dissociative recombination starts to dominate. For the higher pressure considered here (4 torr) this channel dominates for Ar percentages between 5% and 95%. The observed increase in the relative number of ground state N(^{4}S) atoms at high Ar percentage ($>50\%$), for all the pressures considered, can be attributed to the increasing contribution of recombination as shown in the figure. At lower Ar fractional percentages, the dissociation degree variation follows the changes in the high energy part of the electron energy distribution function [10]. In conclusion, these results clearly

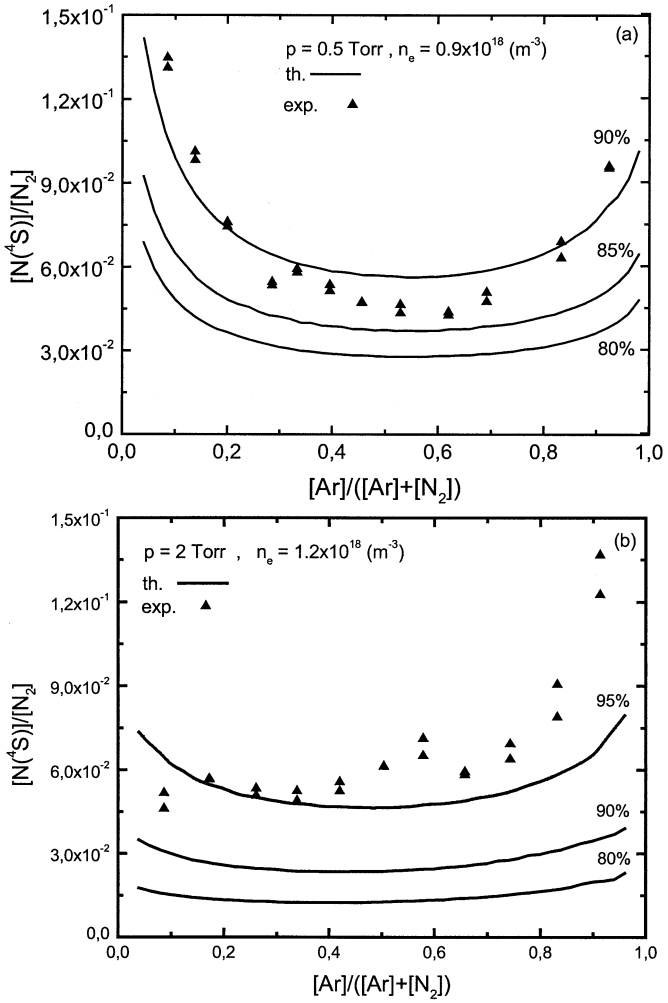

Fig. 14. (a), (b) Variation of ground state atom relative number $[N(^4S)]/[N_2]$ with Ar fractional concentration for various percentages of destruction of metastable atoms back to $N(^4S)$ ground state.

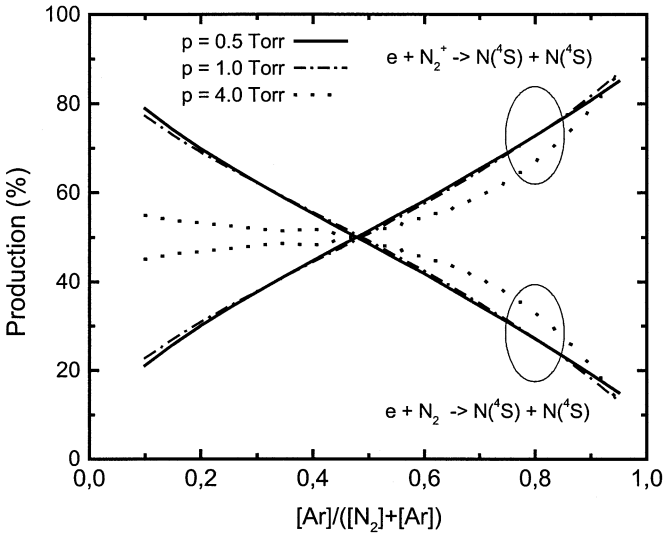

Fig. 15. Relative contribution of the $N(^4S)$ source channels ($\omega/2\pi = 2.45$ GHz, $R = 0.7$ cm).

show that changes in the Ar percentage can be used to control and enhance the degree of N_2 molecular dissociation.

IV. Conclusion

We have presented an investigation of the dissociation processes in low pressure H_2, N_2, and N_2–Ar microwave discharges sustained by traveling surface waves in which the coupling between electron, vibrational and chemical kinetics, wave electrodynamics and plasma—wall interactions is consistently taken into consideration. By applying emission spectroscopy, experimental validations of the model predictions have been performed. From the comparison between theoretical and experimental results, the following main conclusions about H_2 and N_2 molecular dissociation in surface wave sustained microwave discharges can be drawn:

1) The dissociation kinetics in a pure H_2 discharge is mainly determined by electron impact dissociation and wall reassociation of H(1s) atoms into H_2 molecules for the low pressure conditions considered. Molecular dissociation of H_2 molecules is strongly influenced by the value of the wall loss probability, which depends heavily on the wall conditions, in particular on the wall temperature. This dependence can be used to achieve an external dynamic control of hydrogen dissociation.
2) The results for pure N_2 discharges demonstrate the existence of strong correlation between the kinetics of $N(^4S)$, $N(^2D)$, and $N(^2P)$ atoms and $N_2(A^3\Sigma_u^+)$ metastables through the reactions:

$$\mathrm{e} + \mathrm{N}(^4\mathrm{S}) \leftrightarrow \mathrm{e} + \mathrm{N}(^2\mathrm{D})$$
$$\mathrm{e} + \mathrm{N}(^4\mathrm{S}) \leftrightarrow \mathrm{e} + \mathrm{N}(^2\mathrm{P})$$
$$\mathrm{N}(^4\mathrm{S}) + \mathrm{N}_2(\mathrm{A}^3\Sigma_u^+) \rightarrow \mathrm{N}_2(\mathrm{X}^1\Sigma_g^+, 6 \le v \le 9) + \mathrm{N}(^2\mathrm{P})$$
$$\mathrm{N}_2(\mathrm{X}^1\Sigma_g^+, v \ge 10) + \mathrm{N}(^2\mathrm{P}) \rightarrow \mathrm{N}(^4\mathrm{S}) + \mathrm{N}_2(\mathrm{A}^3\Sigma_u^+)$$

3) Ar atoms strongly influence the dissociation processes of N_2 in N_2–Ar discharges at the high degrees of ionization achieved in microwave discharges. Positive N_2^+ ions are the dominant positive charged particles over a wide range of Ar percentages. This is a consequence of the contribution of the charge transfer processes between Ar^+ and N_2 and of the effective associative ionization involving $N_2(A^3\Sigma_u^+)$ metastables. The increase in the relative number of ground state $N(^4S)$ atoms at high Ar fractional percentages can be attributed to dissociative recombination of N_2^+ with electrons.

In conclusion, surface wave sustained discharges operating at microwave frequencies are promising sources of ground state atoms [$N(^4S)$, H(1s)] as the results demonstrate. However, the kinetics of gas discharges in molecular gases is a complex subject due to the highly nonlinear reaction processes occurring simultaneously that strongly affect the nonequilibrium discharge kinetics. For this reason, it is essential to combine theoretical and experimental investigations in order to reveal the main kinetics mechanisms, in particular those of the dissociation kinetics. Unfortunately, the predictions of the models rely heavily on the data used for different processes and in many cases data is still not known with sufficient accuracy. This lack of knowledge is particularly crucial for plasma-wall interactions, a major difficulty being that such interactions depend heavily on the wall conditions. For this reason, much theoretical and experimental

work still needs to be done in order to improve knowledge on *atom* $\leftrightarrow$ *wall* interactions.

REFERENCES

[1] C. M. Ferreira, F. M. Dias, and E. Tatarova, "Travelling wave discharges in nitrogen: Modeling and experiment," in *Advanced Technologies Based on Wave and Beam Generated Plasmas*. Norwell, MA: Kluwer, 1999, pp. 311–334.

[2] H. Sugai, I. Ghanashev, and M. Nagatsu, "High-density flat plasma production based on surface waves," *Plasma Sources Sci. Technol.*, vol. 7, pp. 192–205, 1998.

[3] A. Ricard, J. E. Oseguera-Pena, L. Frank, H. Michel, and M. Gantois, "Active species in microwave postdischarge for steel surface nitriding," *IEEE Trans. Plasma Sci.*, vol. 18, pp. 940–944, Dec. 1990.

[4] P. Merel, M. Tabbal, M. Chaker, M. Moisan, and A. Ricard, "Influence of the field frequency on the nitrogen atom yield in the remote plasma of an N_2 high frequency discharge," *Plasma Sources Sci. Technol.*, vol. 7, pp. 550–556, 1998.

[5] M. Capitelli, C. M. Ferreira, B. F. Gordiets, and A. I. Osipov, *Plasma Kinetics in Atmossperic Gases*. Berlin, Germany: Springer-Verlag. 200.

[6] B. Gordiets, C. M. Ferreira, M. J. Pinheiro, and A. Ricard, "Self-consistent kinetic model of low-pressure N_2-H_2 flowing discharges: I. Volume processes," *Plasma Sources Sci. Technol.*, vol. 7, pp. 363–378, 1998.

[7] ——, "Self-consistent kinetic model of low-pressure N_2-H_2 flowing discharges: II. Surface processes and densities of N, H; NH_3 species," *Plasma Sources Sci. Technol.*, vol. 7, pp. 379–388, 1998.

[8] E. Tatarova, F. M. Dias, C. M. Ferreira, and A. Ricard, "On the axial structure of a nitrogen surface wave sustained discharge: Theory and experiment," *J. Appl. Phys.*, vol. 85, pp. 49–62, 1999.

[9] V. Guerra, E. Tatarova, F. M. Dias, and C. M. Ferreira, "On the self-consistent modeling of a travelling wave sustained nitrogen discharge," *J. Appl. Phys.*, vol. 91, pp. 49–62, 2002.

[10] J. Henriques, E. Tatarova, V. Guerra, and C. M. Ferreira, "Wave driven N_2–Ar dicharge: I self-consistent model," *J. Appl. Phys.*, vol. 91, pp. 5622–5631, 2002.

[11] ——, "Wave driven N_2–Ar dicharge: II experiment and comparison with theory," *J. Appl. Phys.*, vol. 91, pp. 5632–5639, 2002.

[12] F. M. Dias, E. Tatarova, and C. M. Ferreira, "Spatially resolved experimental investigation of a surface wave sustained discharge in nitrogen," *J. Appl. Phys.*, vol. 83, pp. 4602–4609, 1998.

[13] C. M. Ferreira, B. F. Gordiets, and E. Tatarova, "Kinetic theory of low-temperature plasmas in molecular gases," *Plasma Phys. Control. Fusion*, vol. 42, pp. B165–B188, 2000.

[14] E. Tatarova, F. M. Dias, C. M. Ferreira, V. Guerra, J. Loureiro, E. Stoykova, I. Ghanashev, and I. Zhelyazkov, "Self-consistent kinetic model of a surface-wave sustained discharge in nitrogen," *J. Phys. D: Appl. Phys.*, vol. 30, pp. 2663–2676, 1997.

[15] B. Gordiets, M. Pinheiro, E. Tatarova, F. M. Dias, C. M. Ferreira, and A. Ricard, "A travelling wave sustained hydrogen discharge: Modeling and experiment," *Plasma Sources Sci. Technol.*, vol. 9, pp. 295–303, 2000.

[16] V. Guerra and J. Loureiro, "Non-equilibrium coupled kinetics in stationary N_2-O_2 discharge," *J. Phys. D: Appl. Phys.*, vol. 28, pp. 1903–1918, 1995.

[17] R. S. Freund, R. C. Wetzel, and R. J. Shul, "Measurements of electron-impact-ionization of N_2, CO, CO_2, CS, CS_2, and metastable N_2," *Phys. Rev. A*, vol. 41, pp. 5861–5868, 1990.

[18] D. Levron and A. V. Phelps, "Quenching of $N_2(A^3\Sigma_u^+, v = 0, 1)$by N_2, Ar, and H_2," *J. Chem. Phys.*, vol. 69, pp. 2260–2262, 1978.

[19] J. Bacri and A. Medani, "Electron diatomic molecule weighted total cross section calculation," *Physica B + C*, vol. 112, pp. 101–118, 1982.

[20] D. Rapp and P. Englander-Gold, "Total cross sections for ionization and attachment in gases by electron impact: I. Positive ionization," *J. Chem. Phys.*, vol. 43, pp. 1464–1479, 1991.

[21] V. Guerra and J. Loureiro, "Electron and heavy particles kinetics in a low pressure nitrogen glow discharge," *Plasma Sources Sci. Technol.*, vol. 6, pp. 361–372, 1997.

[22] I. A. Kossyi, A. Yu Kostinsky, A. A. Matveyev, and V. P. Silakov, "Kinetic scheme of the nonequilibrium discharge in nitrogen-oxygen mixture," *Plasma Sources Sci. Technol.*, vol. 1, pp. 207–220, 1992.

[23] T. F. O'Malley, A. J. Cunninham, and R. M. Hobson, "Dissociative recombination at elevated temperatures. II comparison between theory and experiment in neon and argon afterglows," *J. Phys. B.*, vol. 5, pp. 2126–2133, 1972.

[24] A. B. Sa, "Modelização de Plasmas Produzidus por Ondas de Superfície," Ph.D. thesis, Instituto Superior Técnico, Tech. Univ. of Lisbon, Lisbon, Portugal , 1989.

[25] R. Fafari, "Descharges micro-ondes en ecoulement dans les melanges oxygene-azote comme sources d'oxygene atomique et singulet. Comparison a d'autres types de plasmas," Ph.D. thesis, Universite Paris-Sud, Orsay, France, 1992.

[26] F. M. Dias, E. Tatarova, J. Henriques, and C. M. Ferreira, "Surface wave propagation in collisional plasma columns," *J. Appl. Phys.*, vol. 85, pp. 2528–2553, 1999.

[27] S. Chung and C. C. Lin, "Application of the close-coupling method to excitation of electronic states and dissociation of H_2 by electron impact," *Phys. Rev.*, vol. A17, pp. 1874–1891, 1978.

[28] B. P. Lavrov, "O roli dissociativnogo vozbujdenia v zaselenii atomnih uroven v vodorodnoj plasma s maloj stepeni dissociacii," *Opt. Spectrosc.*, vol. 42, pp. 447–450, 1977. Russian.

[29] J. Loureiro and C. M. Ferreira, "Electron and vibrational kinetics in the hydrogen positive column," *J. Phys. D: Appl. Phys.*, vol. 22, pp. 1680–1691, 1989.

[30] T. Amano, "The dissociative recombination rate coefficients of H_3^+, HN_2^+, and NCO^+," *J. Chem. Phys.*, vol. 92, pp. 6492–6501, 1990.

[31] P. J. Eenshuistra, J. M. Bonnie, J. Los, and H. J. Hopman, "Observation of exceptionally high vibrational excitation of hydrogen molecules formed by wall recombination," *Phys. Rev. Lett.*, vol. 60, pp. 341–344, 1988.

[32] Y. C. Kim and M. Boudart, "Recombination of O, N, and H atoms on silica: Kinetics and mechanism," *Langmuir*, vol. 7, pp. 2999–3005, 1991.

[33] A. M. Devyatov, V. A. Kalinin, and S. D. Mijovich, "Ocenka stepeni dosociacii v vodorodnoi plasma nizkogo davlenia po izmerennie otnosheniam intenzivnostej H_2 fulherovoj $\alpha(d^3\Pi_u - a^3\Sigma_g)$ sistemi i H_α linii," *Optica i Spectroscopia*, vol. 71, pp. 910–913, 1991. Russian.

[34] B. P. Lavrov, V. H. Ostrovsky, and V. I. Ustinov, "Non franc-condon transitions in the electron impact excitation of molecules II. Semi-empirical approach: Transitions in H_2," *J. Phys. B: At. Mol. Phys.*, vol. 14, pp. 4701–4718, 1981.

[35] E. Tatarova, F. M. Dias, and C. M. Ferreira, "Effects of plasma-wall interaction in a wave driven H_2 discharge," in *Proc. 15th Int. Symp. Plasma Chem.*, vol. VI, A. Bouchoule, J. M. Pouvesle, A. L. Thomann, J. M. Bauchire, and E. Robert, Eds., Orleans, France, 2001, pp. 2269–2274.

[36] K. A. Berington, P. G. Burke, and W. B. Robb, "The scattering of electrons by atomic nitrogen," *J. Phys. B: At. Mol. Phys.*, vol. 8, pp. 2500–2511, 1975.

[37] T. G. Black, R. I. Sharpless, and T. G. Stanger, "Measurements of vibrationally excited molecules by Raman scattering. I. The yield of vibrationally excited nitrogen in the reaction $N + NO \rightarrow N_2 + O$," *J. Chem. Phys.*, vol. 38, pp. 4792–4797, 1993.

[38] K. A. Vereshchagin, V. V. Smirnov, and V. A. Shakhatov, "CARS study of the vibrational kinetics of nitrogen molecules in the discharge and afterglow stages of a pulsed discharge," *Tech. Phys.*, vol. 42, pp. 487–494, 1997.

[39] G. Cernogora, "Etude des etats metastables de l'azote atomique dans des discharges lumininescentes," Ph.D. thesis, Universite de Paris-Sud, Orsay, France, 1980.

[40] A. A. Viggiano and R. A. Morris, "Rate constants for the reaction of $Ar^+(^2P_{3/2})$ with N_2 as a function of N_2 vibrational temperature and energy level," *J. Chem. Phys.*, vol. 99, pp. 3526–3530, 1993.

[41] S. Kato, J. A. De Gouw, C. D. Lin, V. M. Bierbaum, and St. R. Leone, "Charge transfer rate constants for $N_2^+(v = 0$–$4)$ with Ar at thermal energies," *Chem. Phys. Lett.*, vol. 256, pp. 305–311, 1996.

Carlos M. Ferreira was born on the June 27, 1948, in Lisbon, Portugal. He graduated in electrical engineering from the Instituto Superior Técnico (IST), Lisbon University of Technology, Lisbon, Portugal, in 1971 and the Doctorat d'Etat degree in physics from the University of Paris XI, Orsay, France in 1976.

He is a Full Professor of Physics at IST and has served as its President since 2001. He formerly served as Vice-President for Science of IST, in 1999–2000, as a Member of the Executive Committee and Council, European Physical Society, in 1992–1997 and 1989–1995, respectively, and as the Secretary-General of the Portuguese Physical Society, in 1990–99. He is a member of the Academia Europaea. His main research interests are in the fields of gas discharges and gaseous electronics, in which he has authored about 200 scientific papers and two books and edited two books. He presented numerous invited papers at major conferences in Europe and the United States.

Elena Tatarova was born in Bulgaria. She received the M.Sc. degree in engineering physics and the Ph.D. degree in plasma physics from Sofia University, Sofia, Bulgaria, in 1980 and 1989, respectively.

She was a Lecturer in the Radiophysics and Electronics Department, Faculty of Physics, Sofia University, in 1989–2000. In 1998–2002, she was an Invited Researcher with the Centro de Fisica dos Plasmas, Instituto Superior Tecnico, Portugal, under a fellowship of the PRAXIS XXI Programme of the Portuguese Ministry of Science and Technology. Presently, she is a Researcher with the Centro de Fisica dos Plasmas, Instituto Superior Tecnico, Portugal. Her current research work is concentrated on complex, theoretical, and experimental investigation of microwave discharges operating in molecular gases including numerical modeling and plasma diagnostic.

Dr. Tatarova was awarded a DAAD scholarship to Ruhr University, Bohum, Germany, in 1993. In 1996, she was awarded a NATO scholarship to the Center of Electrodynamics, Technical University, Lisbon, Portugal.

Vasco Guerra was born in torres Vedras, Portugal, on December 12, 1968. He graduated in physical engineering and received the Ph.D. degree from the Instituto Superior Técnico (IST), Lisbon Technical University, Lisbon, Portugal, in 1991 and 1998, respectively.

Since 1998, he has an been Assistant Professor in the Physics Department of IST. His research interests are focused on the modeling of kinetic processes in molecular plasmas, including electron and heavy-particle kinetics and gas-surface processes.

Boris F. Gordiets was born in Chelabinsk, Russia, on September 23, 1941. He graduated as a engineer-physicist in 1963 from Moscow Physical-Technical Institute, Dolgoprudniy, Russia and received the Candidate of Science and Doctor of Science degrees in 1968 and 1982, respectively.

Since 1968, he has been with the P.N. Lebedev Physical Institute, Russian Academy of Sciences, Moscow, Russia, where he has been a Leading Scientist since 1986. He was an Invited Professor and Researcher in the Instituto Superior Técnico, Lisbon, Portugal. He is currently a Visiting Professor-Investigator at Barcelona University, Barcelona, Spain. His scientific interest is in theoretical investigations and modeling of kinetic processes in molecular physics, physics of gas lasers, atmospheric and ionospheric optics, and low-temperature plasma.

Júlio Henriques was born in Lisbon, Portugal, on March 7, 1970. He received graduated in physics engineering from the Faculty of Science and Technology, New University of Lisbon, Lisbon, Portugal, in 1995 and the M.Sc. and Ph.D. degrees in 1998 and 2002, respectively, from the Instituto Superior Técnico (IST), Lisbon Technical University, Lisbon, Portugal, where he is currently pursuing the Post-Doc at IST.

He is currently with the Centro de Física dos Plasmas, Instituto Superior Técnico, Lisbon, Portugal. His research interests are in gas electronics, atomic and molecular processes in plasmas, kinetic theory, and modelization of wave-driven discharges.

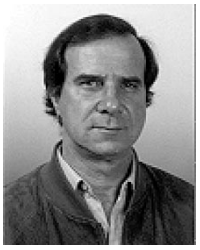

Francisco M. Dias was born in Portimão, Portugal, on March 28, 1949. He graduated in electrical engineering from the Instituto Superior Técnico (IST), Lisbon Technical University, Lisbon, University, in 1971, and the research degree equivalent to the Ph.D. degree in physics from the Instituto Nacional de Investigaçáo Cientifica, in 1988.

Since 1972, he has been a Researcher at IST and became Investigador Principal in 1997. From 1974 to 2002, he lectured propagation and radiation of electromagnetic waves at the Military Academy where he became Associated Professor in 1991. He has been working in hollow cathode arcs and surface wave discharges, and his main research interests concern plasma diagnostics.

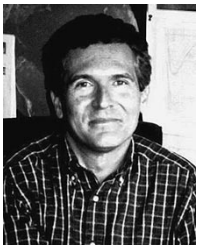

Mário Pinheiro was born in Lço. Marques (now Maputo), Mozambique. He received the physics degree in 1986 and the Diplôme d' Études Approfondies in plasma physics from the University of Orsay, Orsay, France, in 1987.

He prepared his Ph.D. thesis at the Instituto Superior Técnico, Lisbon, in the Group of Prof. C. M. Ferreira, and in close cooperation with Gerard Gousset, from LPGP, Orsay. He is currently with the Centro de Física dos Plasmas, Instituto Superior Técnico, Lisbon, Portugal. His main research interests are in the study of the gas discharge structure and plasma propulsion.